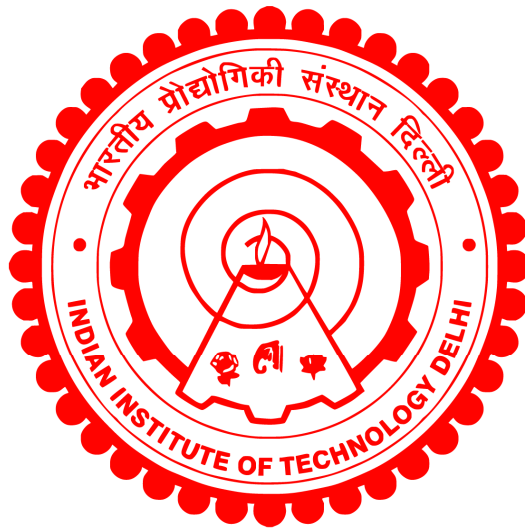


**EXPERIMENTS AND SIMULATIONS OF  
SCRATCH ON BARE AND 2D MATERIAL-  
PROTECTED SILICA GLASS**

**SOURAV SAHOO**



**DEPARTMENT OF MATERIALS SCIENCE AND ENGINEERING  
INDIAN INSTITUTE OF TECHNOLOGY DELHI  
SEPTEMBER 2024**

**Indian Institute of Technology Delhi (IITD), New Delhi, 2024**

# **EXPERIMENTS AND SIMULATIONS OF SCRATCH ON BARE AND 2D MATERIAL- PROTECTED SILICA GLASS**

by

**Sourav Sahoo**

Department of Materials Science and Engineering

Submitted in fulfillment of requirements of the degree of

Doctor of Philosophy

to the

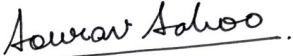


**INDIAN INSTITUTE OF TECHNOLOGY DELHI**

**SEPTEMBER 2024**

# Declaration

I hereby declare that the thesis contains the work carried out in fulfillment of the requirements for the award of the degree of Doctor of Philosophy under the guidance and supervision of **Prof. Nitya Nand Gosvami**, Associate Professor, Department of Materials Science and Engineering, and **Prof. N. M. Anoop Krishnan**, Associate Professor, Department of Civil Engineering & Yardi School of Artificial Intelligence, Indian Institute of Technology Delhi. The contents of the dissertation, including text, tables, and figures, have not been reproduced from other reports, theses, etc. Wherever reproduction has been made from books, journals, reports, manuals, websites, etc., the corresponding sources have been duly acknowledged and referenced appropriately.



Sourav Sahoo

September 2024

# Certificate

This is to certify that the thesis entitled “*Experiments and Simulations of Scratch on Bare and 2D Material-Protected Silica Glass*” is being submitted by **Mr. SOURAV SAHOO** to the Indian Institute of Technology Delhi for the award of the degree of **DOCTOR OF PHILOSOPHY**. This is a record of the bonafide research work entirely carried out by him under our supervision and guidance. The matter presented in this thesis has not been submitted, in part or in full, to any other University or Institute for the award of any degree or diploma.



**Prof. Nitya Nand Gosvami**

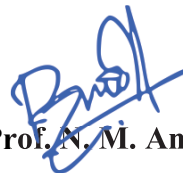
Associate Professor,

Department of Materials Science and Engineering,

Indian Institute of Technology Delhi,

Hauz Khas, New Delhi-110016.

September 2024



**Prof. N. M. Anoop Krishnan**

Associate Professor,

Department of Civil Engineering & Yardi

School of Artificial Intelligence,

Indian Institute of Technology Delhi,

Hauz Khas, New Delhi-110016.

September 2024

# Acknowledgments

First and foremost, I express my sincere appreciation to my supervisors, Prof. Nitya Nand Gosvami and Prof. N. M. Anoop Krishnan, for their guidance that provided direction to my magnitude of efforts. My transition from a directionless bachelor's student to a dedicated scientific scholar was largely inspired by their professionalism. This dissertation would not have been possible without their constant encouragement and timely corrections, which helped keep my progress on track. Additionally, I would like to thank the SRC members—Prof. Rajesh Prasad, Prof. Jayant Jain, and Prof. Shashank Bishnoi, for their invaluable feedback and critical evaluations of my research. Also, I extend my deepest gratitude to my collaborators—Dr. Om Prakash Khatri (CSIR-IIP), Prof. Zhijiang Ye (Miami University), Prof. Viswanath Balakrishnan, and Dr. Deepa Thakur (IIT Mandi) for lending their expertise which significantly contributed to the success of this dissertation's projects. Further, I am grateful to Prof. Philip Egberts and Dr. Chaochen Xu (University of Calgary) for their helpful inputs on graphene exfoliation.

The social fabric of one's life is incomplete without family, of both blood and brethren. To this, I sincerely thank my parents, Mr. Ganesh Chandra Sahoo and Mrs. Manju Bala Sahoo, for all their unconditional support throughout my life and this doctoral journey, in particular. Nothing can ever compensate for the time spent away from them during my academic endeavors. Their silent patience amidst all the calls missed, conversations cut short, and vacations canceled is highly appreciated. Their inherent understanding of my priorities has been the foundation of all my personal and professional liberties over the years. All the privileges I endow, and every achievement I own are dedicated to them. I further acknowledge my sibling, Ms. Smruti Sahoo, and my brother-in-law, Mr. Aditya Kunal, for their care and support despite their busy work schedules. Surviving homesickness was only possible because they pampered me with their culinary skills and made me feel welcome at their beautiful place, which is the closest to home I have had here.

Commendations are devoted to the NTM3 and M3RG lab fraternity for promoting a healthy work environment and serving as the first critic and feedback panel of my work. From being a newcomer to becoming a seasoned member integrated into the multi-disciplinary community, I owe my growth and transition to all my lab colleagues. Firstly, I acknowledge Dr. S. Kasimuthumaniyan for his unparalleled mentorship and camaraderie throughout my doctoral research. Our countless hours spent discussing politics, cricket, and movies provided the

escapism we both needed. In addition, I thank Ms. Shweta Rani Keshri, Mr. Sajid Mannan, and Mr. Indrajeet Mandal for being the amicable colleagues comprising the "Glass Group." With the mixed bag of expertise they possess, any sort of help was just a call (and a treat) away.

Thanks are also extended to Dr. Himanshu Rai and Mr. Jitendra Soni for their constructive feedback and productive discussions about AFM, tribology, and life, in general. I have learned more technicalities of AFM from our mutual communications than from any classical textbook—the innumerable scribblings in Jitendra's journal serve as a testament to that! Special thanks to Mr. Surajbhan Jaiswal for always finding time for coffee/ice-cream breaks and impromptu dinners, which allowed me to get to know him better than during our undergraduate days together. I further thank my other labmates and colleagues—Dr. Ravinder, Dr. Rajesh Kumar, Dr. Amreen Jan, Dr. Priyanka Saini, Ms. Tanu Pittie, Mr. Ashish Yadav, Mr. Mohd Zaki, Mr. Syed Junaid, Mr. Debottam Datta, Mr. Suresh, Mr. Sanchit Bedi, Mr. Sheikh Junaid Fayaz, Mr. Vaibhav Bihani, and Mr. Vishal Bhaskar for their valuable contributions at different stages of this Ph.D. journey. Research is not a solo venture; Thanks to all the innumerable colleagues and friends across multiple labs and departments whose contributions fit the scope of this section.

A significant portion of one's Ph.D. involves dealing with purchases and administrative paperwork; Thanks to Mr. Deepak R. Chaubey, Lab Manager, M3RG, for sparing me the trouble and coordinating with my work requirements. I also acknowledge the staff of the DMSE office—Mr. Amit Kumar, Ms. Sahlini Arora, Ms. Sunita Rani, and Mr. Ramesh Kr. Pandey for the smooth and timely processing of my documents without any prompts. Additionally, I would like to thank Mr. Brijesh K. Sah and Mr. S. B. Prasad (Lab-in-charge, DMSE), and Mr. Mukund Shastry (Project Staff, DMSE/FITT) for their help and suggestions in designing some of my crucial experiments.

I consider myself fortunate to have worked with a few talented undergraduates who not only excelled in their research roles but also have been great companions outside research. Special mentions go to Mr. Utkarsh Tiwari and Mr. Romit R. Kaware for being the pioneers of this batch and for their appreciable work in establishing the pipelines of scratch simulations right from "scratch!" In the realm of experiments, I solemnly acknowledge the work done with and by Ms. Zuhaa Khan during her time as an exchange student which emerged as the most timely and significant addition to my dissertation. If not for her, the project would have been only half as impactful as it turned out to be. Additionally, I extend my indebtedness to Ms. Vernika

Gautam for our brief but highly productive internship project, and Mr. Manish Verma for implementing his ingenious mathematical rigor and coding faculties to our research problems. I feel proud that all of them have contributed as an author in the publications stemming from their respective projects with me.

Last but not least, I acknowledge and dedicate this dissertation to myself. To all the times, easy and tough, and to all the triumphs, heartbreaks, and breakdowns that have led me to the completion of this long but beautiful journey—I hope it was all worth it.

# Abstract

The ubiquitous presence of glasses in our daily lives emphasizes their importance, yet their susceptibility to contact damage, such as indents and scratches, remains a significant drawback. Specifically, a scratch encompasses a larger vicinity on the glass surface, leaving behind a trail of micro-crack defects. These scratch-induced defects further act as nucleation centers for mechanical fracture and atmospheric corrosion, both of which are detrimental to the functionality and life of a glass product. Hence, understanding the mechanisms of glass deformation preceding scratch-associated flaw formation is vital to developing better scratch-resistant glasses. To this extent, this dissertation focuses on investigating the structural changes in the amorphous silica network accompanying shear and explores the burgeoning potential of atomically thin two-dimensional (2D) materials in enhancing scratch damage resistance.

Ideally, 2D material-based coatings seem like a perfect candidate for protecting glasses—they are atomically thin and minimally affect the transparency and mechanical tolerances; their flexibility allows for conformal contact with the glass substrate, promoting higher adhesion; and the weak van der Waals forces enable easy shearing against sliding counterfaces. Moreover, specific 2D materials such as graphene are known to be chemically impermeable and act as stable barrier layers to both liquids and gases. Additionally, the chemical inertness and thermal stability of graphene render it durable in environmentally extreme conditions. Nevertheless, the applicability of such 2D coatings is hindered by uniform, large-area, and high-quality deposition requirements and is inadequately explored for glass substrates.

First, employing atomistic simulations and multiscale experiments, the scratch damage of silica glass is examined. The glass surface is pre-indented to a constant depth and then dragged to simulate a linear scratch, and the structural impact in the indent-to-scratch transitioning phase is examined. It is observed that despite the differences in length and timescales, the simulated values of indentation hardness and coefficient of friction (COF) exhibit excellent agreement with experimental values from nanoindentation and atomic force microscopy (AFM) experiments, respectively. Interestingly, analysis of the subsurface deformation in the scratched region reveals densification and shear flow, in contrast to pure densification, as in the case of indentation. Furthermore, similar volume recovery percentages from experiments and simulation reveal that the reversible component of plastic deformation owing to densification is comparable in both cases. Finally, in contrast to the common hypothesis, it is demonstrated that while the bond angles recover, the medium-range ring structure does not recover upon

annealing, although they exhibit some relaxation. Overall, this study sheds new light on the crucial role of the medium-range structure of glasses subjected to scratch deformation.

Next, it is shown that the interfacial friction and wear on glasses during scratch in a liquid environment can be significantly reduced using aqueous graphene oxide (GO) dispersion. This is made possible by the in situ tribological generation of a GO-derived film from its dispersion during the repeated scratching of silica glass. The formation of the dense GO tribofilm on the scratch track is confirmed by micro-Raman spectroscopy and AFM analysis. Interestingly, the lubricious GO tribofilm is observed to reduce the frictional forces by ~80% compared to pure water. This reduced friction, in turn, limits the shear-induced tensile stresses in the vicinity of sliding contact, thereby minimizing the density of partial Hertzian cone cracks. The optical micrographs confirm the contrasting crack density and wear severity in conjunction with the protective GO tribofilm. Furthermore, the effect of frictional forces on the wear and cracking behavior is established theoretically to highlight friction's role in determining the extent of damage. Overall, this study shows that the scratch resistance of glass surfaces in aqueous conditions could be significantly enhanced through a hitherto unknown tribofilm generation mechanism.

In the following study, it is demonstrated that silica glasses protected with mechanically exfoliated few-layer graphene sheets can exhibit a remarkable improvement in scratch and tribocorrosion resistance. The friction and wear characteristics of graphene-coated silica glasses are evaluated at the nanoscale with AFM-based scratch experiments in dry and wet conditions. For the dry case, the friction forces recorded while scratching the graphene-glass surfaces against diamond tips exhibit ~98% reduction compared to the bare silica glass, with the COF falling in the superlubric regime. This superlubricity, combined with the stress-shielding nature of graphene, shifts the glass damage mode from aggressive plastic plowing to milder densification-type deformations, as corroborated by atomistic simulations. Further, the graphene-glasses are scratched in water to study the environmental influence on friction and wear. Intriguingly, in wet conditions, graphene is shown to enhance the resistance to not only the mechanical damages with inert diamond tips but also against mechanochemical wear occurring with chemically reactive Si-DLC tips. The chemical pathways of hydration and tribocorrosion interactions at the glass interface are evaluated with reactive simulations, which establish the chemical passivity of graphene protecting against tribochemical wear. Altogether, this work provides a new fillip for developing glasses with enhanced scratch and tribocorrosion resistance exploiting graphene coatings.

Finally, the possibility of depositing and employing large-area 2D films of WS<sub>2</sub> as anti-scratch coatings for glass substrates is investigated. Nanometer-thick monolayers of WS<sub>2</sub> are uniformly grown on silica glass with minimal topographic and chemical heterogeneity via the chemical vapor deposition (CVD) method. Nanoscale AFM scratch experiments reveal a notable ~95% reduction in the COF with WS<sub>2</sub>, although being almost twice as high as graphene. However, unlike graphene, the rupture and delamination endurance of WS<sub>2</sub> films is found to be distinguishably high. Further, the scratch morphology on WS<sub>2</sub>-glass indicates no plowing damage but rather a weak non-wear distortion that is ~75% lower than that on graphene-glass. Similar to graphene, this structural distortion is revealed to be of the densification type with atomistic simulations. Interestingly, it is seen that the WS<sub>2</sub> monolayer can absorb a significant magnitude of stresses, shielding the glass from densification under normal indentation. Only when the indentation is translated to a scratch does the densification set in, implying that the resulting densification is inherently associated with the shearing of bonds. In summary, the objective of the dissertation is to investigate and understand the mechanical and mechanochemical scratch damage of bare and 2D material-coated silica glass at multiple length scales.

## सार

हमारे दैनिक जीवन में कांच की सर्वव्यापी उपस्थिति उनके महत्व पर जोर देती है, फिर भी इंडेंट और खरोंच जैसे संपर्क क्षति के लिए उनकी संवेदनशीलता एक महत्वपूर्ण कमी बनी हुई है। विशेष रूप से, एक खरोंच कांच की सतह पर एक बड़े क्षेत्र को घेर लेता है, जिससे सूक्ष्म-दरार क्षति का निशान पीछे रह जाता है। ये खरोंच-प्रेरित क्षति आगे संरचनात्मक फ्रैक्चर और वायुमंडलीय क्षरण के लिए न्यूक्लियेशन केंद्रों के रूप में कार्य करती हैं, जो दोनों एक कांच उत्पाद की कार्यक्षमता और जीवन के लिए हानिकारक हैं। इसलिए, बेहतर खरोंच-प्रतिरोधी कांच के विकास के लिए खरोंच से संबंधित क्षति निर्माण से पहले कांच विरूपण के तंत्र को समझना महत्वपूर्ण है। इस हद तक, यह शोध प्रबंध अपरूपण के साथ अमोर्फोस सिलिका नेटवर्क में संरचनात्मक परिवर्तनों की जांच करने पर केंद्रित है और खरोंच क्षति प्रतिरोध को बढ़ाने में परमाणु रूप से पतले दो-आयामी (2डी) पदार्थ की बढ़ती क्षमता की खोज करता है।

आदर्श रूप से, 2डी पदार्थ-आधारित आवरण कांच की सुरक्षा के लिए एक आदर्श उम्मीदवार की तरह लगता है-वे परमाणु रूप से पतले होते हैं और पारदर्शिता और यांत्रिक सहिष्णुता को न्यूनतम रूप से प्रभावित करते हैं; उनका लचीलापन कांच के सबस्ट्रेट के साथ अनुरूप संपर्क की अनुमति देता है, उच्च आसंजन को बढ़ावा देता है; और कमजोर वैन डेर वाल्स प्रभाव स्लाइडिंग काउंटरफेस के खिलाफ आसान कतरनी को सक्षम करता है। इसके अलावा, ग्राफीन जैसे विशिष्ट 2डी पदार्थ रासायनिक रूप से अभेद्य होने के लिए जाने जाते हैं और तरल और गैसों दोनों के लिए स्थिर बाधा परतों के रूप में कार्य करते हैं। इसके अतिरिक्त, ग्राफीन की रासायनिक अभेद्यता और तापीय स्थिरता इसे पर्यावरण की चरम स्थितियों में टिकाऊ बनाती है। फिर भी, इस तरह के 2डी आवरण की प्रयोज्यता समान, बड़े क्षेत्र और उच्च गुणवत्ता वाले निक्षेपण आवश्यकताओं से बाधित होती है। इसके अलावा, कांच के सबस्ट्रेट के लिए इस तरह के 2डी आवरण पर अपर्याप्त रूप से शोध किया गया है।

सबसे पहले, परमाणु अनुकरण और बहुस्तरीय प्रयोगों को नियोजित करते हुए, सिलिका ग्लास के खरोंच क्षति की जांच की गई है। कांच की सतह को एक निरंतर गहराई तक पूर्व-इंडेंट किया जाता है और फिर एक रैखिक खरोंच का अनुकरण करने के लिए खींचा जाता है, और इंडेंट-टू-स्क्रैच परिवर्तन के दौरान संरचनात्मक प्रभाव की जांच की जाती है। यह देखा गया है कि लंबाई और समय-सीमा में अंतर के बावजूद, इंडेंटेशन हार्डनेस और घर्षण के सैद्धांतिक मूल्य नैनोइंडेंटेशन और परमाणु बल सूक्ष्मदर्शी (ए. एफ. एम.) प्रयोगों के साथ उत्कृष्ट सहमति प्रदर्शित करते हैं। दिलचस्प बात यह है कि खरोंच वाले क्षेत्र में उपसतह विरूपण के विश्लेषण से केवल घनत्व के बजाय घनत्व और अपरूपण प्रवाह दोनों का पता

चलता है। इसके अलावा, प्रयोगों और अनुकरण से समान मात्रा वसूली प्रतिशत से पता चलता है कि घनत्व के कारण प्लास्टिक विरूपण का प्रतिवर्ती घटक दोनों मामलों में तुलनीय है। अंत में, सामान्य परिकल्पना के विपरीत, यह प्रदर्शित किया जाता है कि जब बॉन्ड कोण ठीक हो जाते हैं, तो मध्यम दूरी की रिंग संरचना थर्मल एनीलिंग पर ठीक नहीं होती है, हालांकि वे कुछ हद तक विश्राम प्रदर्शित करते हैं। कुल मिलाकर, यह अध्ययन खरोच विरूपण के अधीन कांच की मध्यम-सीमा संरचना की महत्वपूर्ण भूमिका पर नई रोशनी डालता है।

इसके बाद, यह दिखाया गया है कि जलीय ग्राफीन ऑक्साइड (GO) तरल का उपयोग करके तरल वातावरण में खरोच के दौरान कांच पर अंतरफलक घर्षण और घिसाव को काफी कम किया जा सकता है। यह सिलिका ग्लास के बार-बार खरोचने के दौरान एक GO-व्युत्पन्न परत के इन सीटू ट्राइबोलॉजिकल गठन से संभव हुआ है। खरोच मार्ग पर घने GO ट्राइबोफिल्म के गठन की पुष्टि माइक्रो-रमन स्पेक्ट्रोस्कोपी और ए. एफ. एम. विश्लेषण द्वारा की जाती है। दिलचस्प बात यह है कि स्नेहन GO ट्राइबोफिल्म शुद्ध पानी की तुलना में घर्षण बलों को ~80% तक कम कर देता है। यह कम घर्षण, बदले में, स्लाइडिंग संपर्क के आसपास कतरनी-प्रेरित तन्यता तनाव को सीमित करता है, जिससे आंशिक हर्ट्ज़ियन शंकु दरारों के घनत्व को कम करता है। ऑप्टिकल माइक्रोग्राफ सुरक्षात्मक GO ट्राइबोफिल्म के साथ कम दरारों और घिसाव की पुष्टि करते हैं। इसके अलावा, क्षति की सीमा निर्धारित करने में घर्षण की भूमिका को उजागर करने के लिए घिसाव और दरारों पर घर्षण का प्रभाव सैद्धांतिक रूप से स्थापित किया जाता है। कुल मिलाकर, इस अध्ययन से पता चलता है कि जलीय परिस्थितियों में कांच की सतहों के खरोच प्रतिरोध को एक अज्ञात ट्राइबोफिल्म उत्पादन तंत्र के माध्यम से काफी बढ़ाया जा सकता है।

अगले अध्ययन में, यह दिखाया गया है कि यांत्रिक रूप से एक्सफोलिएटेड कुछ-परत वाली ग्राफीन शीट से संरक्षित सिलिका ग्लास खरोच और ट्राइबोकरोज़न प्रतिरोधन में उल्लेखनीय रूप से सुधार कर सकते हैं। ग्राफीन-संरक्षित सिलिका कांच के घर्षण और घिसाव का मूल्यांकन नैनोस्केल पर परमाणु बल सूक्ष्मदर्शी (ए. एफ. एम.) आधारित खरोच प्रयोगों के साथ शुष्क और गीली परिस्थितियों में किया गया है। सूखे मामले के लिए, डायमंड की नोकों के खिलाफ ग्राफीन-ग्लास सतहों को खरोच करते समय दर्ज किया गया घर्षण नंगे सिलिका ग्लास की तुलना में ~98% की कमी प्रदर्शित करता है, जिसमें घर्षण गुणांक सुपरलुब्रिक रेंज में पड़ता है। यह सुपरलुब्रिसिटी, ग्राफीन की तनाव-परिरक्षण प्रकृति के साथ मिलकर, कांच की क्षति को आक्रामक प्लास्टिक जुताई से हल्के घनत्व-प्रकार की विकृतियों में बदल देती है, जैसा कि परमाणु अनुकरण द्वारा पुष्टि की गई है। इसके अलावा, घर्षण और घिसाव पर पर्यावरणीय प्रभाव का अध्ययन करने के लिए ग्राफीन-ग्लास को पानी में खरोच कर दिया गया है। दिलचस्प रूप से, गीली

परिस्थितियों में, ग्राफीन न केवल निष्क्रिय डायमंड की नोकों के खिलाफ यांत्रिक क्षति प्रतिरोध को बढ़ाता है, बल्कि रासायनिक रूप से प्रतिक्रियाशील Si-DLC नोकों के साथ होने वाले यांत्रिक-रासायनिक घिसाव के प्रतिरोध को भी बढ़ाता है। ग्लास इंटरफेस पर हाइड्रेशन और ट्राइबोकरोज़न इंटरैक्शन के रासायनिक मार्गों का मूल्यांकन प्रतिक्रियाशील सिमुलेशन के साथ किया गया है, जो ट्राइबोकेमिकल घिसाव से बचाने वाले ग्राफीन की रासायनिक निष्क्रियता को स्थापित करते हैं। कुल मिलाकर, यह काम ग्राफीन कोटिंग्स का उपयोग करके बढ़े हुए खरोंच और ट्राइबोकरोज़न प्रतिरोधी कांच के विकास के लिए एक नया प्रोत्साहन प्रदान करता है।

अंत में, कांच के सबस्ट्रेट के लिए एंटी-स्क्रेच कोटिंग्स के रूप में डब्ल्यूएस2 की बड़े क्षेत्र की 2D फिल्मों को विकसित करने और उपयोग करने की संभावना की जांच की जाती है। डब्ल्यूएस2 के नैनोमीटर-मोटे एकल परतों को रासायनिक वाष्प निक्षेपण (सी. वी. डी.) विधि के माध्यम से न्यूनतम स्थलाकृतिक और रासायनिक विषमता के साथ सिलिका ग्लास पर समान रूप से उगाया जाता है। नैनोस्केल एएफएम खरोंच प्रयोगों से डब्ल्यूएस2 के साथ घर्षण में उल्लेखनीय ~95% की कमी का पता चलता है, हालांकि यह ग्राफीन से लगभग दोगुना अधिक है। हालांकि, ग्राफीन के विपरीत, डब्ल्यूएस2 फिल्मों के टूटने और परिसीमन की सहनशक्ति विशिष्ट रूप से अधिक पाई गई है। इसके अलावा, डब्ल्यूएस2-ग्लास की स्क्रेच मॉर्फोलॉजी कोई जुताई क्षति का संकेत नहीं देती है, लेकिन इसके बजाय एक कमजोर गैर-घिसाव वाली विकृति देखी गई है जो ग्राफीन-ग्लास की तुलना में ~75% कम है। ग्राफीन के समान, यह संरचनात्मक विरूपण परमाणु सिमुलेशन से घनत्व प्रकार का पता चलता है। दिलचस्प रूप से, यह देखा गया है कि डब्ल्यूएस2 मोनोलेयर बड़े पैमाने पर तनाव को अवशोषित कर सकता है जो इंडेंटेशन के तहत कांच को घनत्व से बचा सकता है। केवल जब इंडेंटेशन को खरोंच में अनुवादित किया जाता है, तो घनत्व स्थापित होता है, जिसका अर्थ है कि परिणामी घनत्व स्वाभाविक रूप से रासायनिक बंधनों के कतरनी से जुड़ा होता है। संक्षेप में, शोध प्रबंध का उद्देश्य कई लंबाई के पैमाने पर नंगे और 2डी पदार्थ-लेपित सिलिका ग्लास के यांत्रिक और यांत्रिक-रासायनिक खरोंच क्षति की जांच करना और समझना है।

# Table of Contents

<b>Chapter 1 - Introduction.....</b>	<b>1</b>
1.1 Glasses: definition and types.....	1
1.2 Mechanical limitations of glasses .....	4
1.3 Contact damage on glasses – Indentation vs. scratch.....	8
1.4 Improving contact durability of glasses .....	9
1.5 Organization of the thesis.....	11
<b>Chapter 2 - Literature Review .....</b>	<b>13</b>
2.1 Introduction .....	13
2.2 Contact deformation in oxide glasses.....	13
2.3 Scratch at the macroscale .....	17
2.4 Scratch at the nanoscale .....	20
2.5 Scratch at the atomic scale .....	23
2.6 Tribochemical wear of glasses .....	26
2.7 2D materials as coatings on glasses .....	30
2.8 Summary and conclusions.....	34
<b>Chapter 3 - Motivation and Objectives.....</b>	<b>36</b>
3.1 Motivation .....	36
3.2 Objectives.....	38
<b>Chapter 4 - Methodology .....</b>	<b>40</b>
4.1 Introduction .....	40
4.2 Atomistic modeling and simulations .....	40
4.2.1 Introduction .....	40
4.2.2 Glass preparation simulations.....	45
4.2.3 Indentation and scratching simulations .....	47
4.3 Atomic Force Microscopy .....	49
4.3.1 Introduction .....	49
4.3.2 Calibration of normal and lateral forces .....	52
4.3.3 Contact mode imaging.....	55
4.3.4 Nanoscale scratch experiments.....	55
4.4 Nanoindentation .....	57
4.4.1 Introduction .....	57
4.4.2 Nanoindentation-based scratch experiments .....	58

4.5 Tribometry .....	60
4.5.1 Introduction .....	60
4.5.2 Tribometer scratch experiments .....	61
4.5.3 Friction data processing .....	62
4.6 Optical microscopy .....	63
4.7 Micro-Raman spectroscopy .....	64
4.8 Summary .....	65
<b>Chapter 5 - Scratch Deformation Mechanisms in Silica Glass.....</b>	<b>66</b>
5.1 Introduction .....	66
5.2 Methodology .....	67
5.2.1 Experimental specimen preparation .....	67
5.2.2 Thermal treatment of scratched specimens .....	67
5.2.3 Volume analysis of scratched and annealed specimens .....	68
5.2.4 Annealing simulations and analysis .....	68
5.2.5 Ring statistics and conformation analysis .....	69
5.3 Glass preparation and indentation analysis .....	70
5.4 Scratch deformation and friction analysis .....	72
5.5 Annealing recovery of the densified scratch volume .....	76
5.6 Medium-range order analysis .....	80
5.7 Conclusion .....	84
<b>Chapter 6 - Tribological Behavior of Silica Glass in Graphene-Based Aqueous Dispersions .....</b>	<b>86</b>
6.1 Introduction .....	86
6.2 Methodology .....	88
6.2.1 Synthesis and characterization of GO dispersion .....	88
6.2.2 Experimental specimen preparation – Silica glass .....	89
6.2.3 Experimental specimen preparation – SLS glass .....	89
6.2.4 Tribometer scratch experiments on silica glass .....	90
6.2.5 Deposition of GO on SLS glass .....	91
6.2.6 Tribometer scratch experiments on GO-coated SLS glass .....	92
6.3 Chemical and structural characterization of GO .....	92
6.4 Friction of silica glass in water and GO dispersion .....	94
6.5 Characterization of the GO-derived tribofilm on silica glass .....	95
6.6 Surface damage evolution of silica glass during scratching .....	99
6.7 Mechanics of the microwear damage in silica glass .....	103

6.8 Energetics of the surface damage mechanism in silica glass .....	107
6.9 Tribology of GO-coated SLS glass .....	110
6.9.1 Characterization of GO depositions on SLS glass.....	110
6.9.2 Friction and wear performance of GO-coated SLS glass .....	112
6.10 Conclusion.....	115
<b>Chapter 7 - Nanotribology and Tribochemistry of Graphene-Coated Silica Glass.....</b>	<b>117</b>
7.1 Introduction .....	117
7.2 Methodology .....	118
7.2.1 Experimental specimen preparation .....	118
7.2.2 Mechanical exfoliation of graphene on silica glass.....	119
7.2.3 Simulations of water-glass interactions .....	120
7.3 Characterization of mechanically exfoliated graphene on silica glass.....	122
7.4 Nanotribology of graphene-coated silica glass .....	125
7.4.1 Superlubricity and scratch resistance of graphene-glass surfaces .....	125
7.4.2 Simulation of contact damage over graphene-glass surfaces .....	129
7.5 Tribochemistry of graphene-coated silica glass .....	134
7.5.1 Wet scratch tests with diamond tips .....	134
7.5.2 Wet scratch tests with DLC tips .....	137
7.5.3 Simulations of tribochemical interactions .....	141
7.6 Conclusion.....	146
<b>Chapter 8 - Nanotribology of CVD-Grown WS<sub>2</sub>-Coated Silica Glass .....</b>	<b>148</b>
8.1 Introduction .....	148
8.2 Methodology .....	149
8.2.1 CVD growth of WS <sub>2</sub> monolayers on silica glass.....	149
8.2.2 X-ray photoelectron spectroscopy (XPS).....	150
8.3 Characterization of the WS <sub>2</sub> -glass specimen .....	150
8.4 Nanoscale AFM scratch experiments.....	154
8.5 Atomistic simulation of scratch on WS <sub>2</sub> -glass surfaces .....	157
8.6 Conclusion.....	162
<b>Chapter 9 - Conclusions and Future Work .....</b>	<b>164</b>
9.1 Conclusions .....	164
9.2 Future work .....	166
9.2.1 Selection of appropriate 2D materials as glass coatings.....	166
9.2.2 Large scale 2D material fabrication techniques .....	167
9.2.3 Characterization of other functionalities of 2D material-coated glasses.....	167

<b>References .....</b>	<b>169</b>
<b>Appendices .....</b>	<b>198</b>
Appendix 1 .....	198
Appendix 2 .....	203
<b>List of Publications, Patents, and Conferences .....</b>	<b>213</b>
Publications from dissertation work.....	213
Publications outside dissertation work.....	213
Patents applied.....	214
Conferences attended .....	214
<b>Curriculum Vitae .....</b>	<b>217</b>

# List of Figures

**Figure 1.1** Cross-sectional electron micrograph of the surface flaws on a 19th-century stained glass window of the German Cologne Cathedral (Roemich et al., 2008); The schematic of flaw propagation mechanism under external stresses. ....5

**Figure 2.1 (A)** Cross-sectional optical micrograph of the subsurface densification in an indented alkali boroaluminosilicate glass. Reprinted with permission from ref. (Varshneya et al., 2022), Copyright (2022) John Wiley and Sons. **(B)** SEM micrograph of a sharp indent impression in an alkali silicate glass showing the shear pileup formation around the edges. Reprinted with permission from ref. (K. W. Peter, 1970), Copyright (1970) Elsevier.....16

**Figure 2.2 (A)** The distribution of tensile stress  $\sigma$  (relative to the normal stress  $\sigma_0$ ) with position (relative to the contact radius  $ac$ ) on the surface for a range of friction coefficients in the case of elastic sliding with a spherical indenter. Reprinted with permission from ref. (Hamilton, 1983), Copyright (1983) SAGE Publications Ltd. Journals. **(B)** FEM-computed principal stresses on fused silica glass without (top) and with (bottom) friction highlighting the tensile stress intensification at the rear sliding edge. Reprinted with permission from ref. (Suratwala et al., 2019), Copyright (2019) John Wiley and Sons. .... 19

**Figure 2.3** The plastic, cracking, chipping, and microabrasive regimes of scratch damage observed in silicate glasses with linearly increasing loads. Adapted from ref. (Moayedi & Wondraczek, 2017) under CC BY-NC-ND.....20

**Figure 2.4 (A)** Optical micrograph of AFM cantilever and nanoscratch lines, and the schematic illustration of the nano-IR setup used to acquire the chemical spectra from the scratched region. Reprinted with permission from ref. (He, Chen, et al., 2021), Copyright (2021) Elsevier. **(B)** The AFM topography maps (top) of nanoscratch in silica glass before and after annealing, and the corresponding line profiles (bottom) showing the extent of annealing relaxation. Reprinted with permission from ref. (Shen et al., 2016), Copyright (2016) John Wiley and Sons.....22

**Figure 2.5 (A)** Color map showing the distribution of over-coordinated silicon representing the damaged subsurface layers in scratched silica glass. Reprinted with permission from ref. (T. Liu et al., 2017), Copyright (2017) Trans Tech Publications Ltd. **(B)** Surface profiles of the scratch track on alkali aluminosilicate glass made with conical indenters having varying tip apex angles, progressing from a sharp ( $60^\circ$ ) to a blunt ( $136^\circ$ ) geometry. Reprinted with permission from ref. (Y. N. Ahn & Harris, 2020), Copyright (2020) Elsevier. ....25

<b>Figure 2.6 (A)</b> AFM micrographs and line profiles of nanoscale tribochemical wear tracks on soda lime silica glass surfaces made against silica tips at conditions of increasing relative humidity (across) and increasing normal loads (down). Reprinted with permission from ref. (He, Hahn, et al., 2022), Copyright (2022) Elsevier. <b>(B)</b> Simulation snapshots showing the mechanism of interfacial bridging bond formation – (i) initial state, (ii) dehydrogenation of $\text{Si}^1\text{—O}^2\text{H}^3$ , (iii) formation of $\text{Si}^1\text{—O}^2\text{—Si}^4$ bond. Reprinted with permission from ref. (Guo et al., 2020), Copyright (2020) Elsevier. ....	29
<b>Figure 2.7 (A)</b> Photographs comparing the bare borosilicate glass (leftmost) with the graphene-deposited glasses having different sheet thicknesses obtained by increasing the precursor gas amount during CVD growth. Reprinted with permission from ref. (Sun, Chen, Priydarshi, et al., 2015a), Copyright (2015) American Chemical Society. <b>(B)</b> Schematic showing the prevention of water-induced corrosion of silicate glass with graphene coating; the AFM micrographs on right represents the topography of the bare (top) and graphene-coated glass (bottom) after the static corrosion tests in water. Reprinted with permission from ref. (B. Wang et al., 2016a), Copyright (2016) American Chemical Society. ....	33
<b>Figure 4.1</b> Scheme of silica glass structure preparation using the melt-quench technique.....	47
<b>Figure 4.2</b> Schematic of the atomistic simulation model representing the indentation and scratch trajectories for <b>(A)</b> the bare glass, <b>(B)</b> the graphene-glass, and <b>(C)</b> the $\text{WS}_2$ -glass. ...	49
<b>Figure 4.3 (A)</b> Schematic of the components involved in an AFM setup. Reprinted with permission from ref. (Tien et al., 2005), Copyright (2005) IEEE. <b>(B)</b> The effect of the normal (left) and lateral (right) cantilever bending on the laser beam spot position on the four-quadrant photodiode (Mironov, 2004). ....	52
<b>Figure 4.4 (A)</b> Schematic of the nanoscale scratch test in dry (air) and wet (water) ambience, <b>(B)</b> The experimental AFM setup used for nanoscale scratch experiments.....	56
<b>Figure 4.5 (A)</b> Schematic of the nanoindentation-based scratch test. Adapted from ref. (N. Xue et al., 2023) under CC BY 4.0, <b>(B)</b> The components of the universal nanomechanical tester used for scratch experiments.....	59
<b>Figure 4.6</b> Tribometer experimental setup showing the principal components .....	62
<b>Figure 4.7 (A)</b> The optical microscopy setup, <b>(B)</b> Transparent 500 $\mu\text{m}$ grids attached to the bottom side of the glass for locating the sites of 2D material deposition, <b>(C)</b> The 20 $\times$ micrograph of the gridded glass containing exfoliated graphene as observed from the AFM optical viewport. ....	64

<b>Figure 4.8</b> The confocal laser micro-Raman spectrometer used for the chemical characterization of graphene and WS <sub>2</sub> .....	65
<b>Figure 5.1</b> Load-displacement (P-h) curve of silica glass recorded during the indentation phase. The grey and black lines represent the raw and time-averaged normal forces, respectively. The red line shows the non-linear fit of the unloading portion of the P-h curve. The inset images show the cross-sectional view during different stages (contact, peak, and unload) of the indentation process.....	71
<b>Figure 5.2</b> The simulated and experimental coefficient of friction values for diamond sliding against silica glass at peak normal loads of 123 nN (simulated, grey color; left and bottom axes) and 325 nN (experimental, red color; right and top axes). .....	73
<b>Figure 5.3</b> (A) The topography of the scratch track highlighting the scratch groove and pileups, (B) Top view of the shear strain map of the scratched surface, (C) Cross-sectional densification map of the scratch track representing the local densities in the subsurface region of pre-indent and drag sites, (D) The cross-sectional view of volumetric strain map beneath the scratch. ..	76
<b>Figure 5.4</b> AFM micrographs (A, B) and simulated color maps (C, D) of the as-scratched and annealed-after-scratched silica glass surfaces, respectively, (E) The O–Si–O (intra-tetrahedral) and Si–O–Si (inter-tetrahedral) bond angle distributions in the as-scratched, annealed-after-scratched, and pristine (non-scratched) silica glasses (The annotated values represent the maximum peak positions), (F) Cross-sectional densification map representing the local densities in the subsurface region of pre-indent and drag sites after annealing.....	79
<b>Figure 5.5</b> Distributions of primitive ring sizes in pristine (non-scratched), as-scratched, and annealed-after-scratched silica glasses. The inset schematic shows the methodology of calculating the area and circumference of a ring to characterize its geometry. ....	81
<b>Figure 5.6</b> Statistical distribution of the area:circumference ratios of the rings characterizing their morphology in the pristine, scratched, and annealed-after-scratched silica glasses. The inset images represent the exemplar ring structure for a particular ratio shown by dotted lines. ....	84
<b>Figure 6.1</b> (A) Steps in the synthesis of GO, (B) Chemical structure of GO.....	89
<b>Figure 6.2</b> Schematic of the tribometer experimental setup designed for reciprocating scratch tests on fused silica glasses in a liquid environment.....	91
<b>Figure 6.3</b> (A) FTIR, (B) zeta potential (inset shows the image of the aqueous GO dispersion), (C) XRD pattern, and (D) electron micrograph of synthesized GO.....	93

<b>Figure 6.4</b> (A) COF with respect to time for different reciprocating scratch test conditions on fused silica glass substrate with sapphire probe in DI water and GO dispersion, (B) Variation of friction coefficient values as a function of the applied normal load in DI and GO environments.....	95
<b>Figure 6.5</b> (A) Micro-Raman spectra of a region inside the scratch track showing the characteristic D and G peaks (inset shows the micrograph at the center of which spectral signals were acquired), (B) Optical micrograph (40x) showing the mapping region along the edge of the track, (C) and (D) Intensity map of the 1360 cm <sup>-1</sup> (D) and 1600 cm <sup>-1</sup> (G) peak signals, respectively, from the corresponding mapping region.....	97
<b>Figure 6.6</b> (A) AFM topographical image showing the wear track obtained after scratching fused silica glass with sapphire probe at 7 N normal load in GO dispersion, (B) AFM friction map of the same region of the wear track showing the frictional contrast between the bare unscratched (left) and scratched (right) portions, (C) Line profiles, collected across the white dotted lines in (A) and (B), illustrating the friction signal and topography as a function of X-distance, (D) three-dimensional optical profilometry image of the GO tribofilm formed within the wear track.....	99
<b>Figure 6.7</b> The optical micrographs (10x) of the reciprocating scratch tracks on fused silica glass at varying test conditions in DI (A, C, E) and in GO (B, D, F) showing the differences in the severity of sliding and density of partial Hertzian cone cracks along the track.....	101
<b>Figure 6.8</b> Plot showing the variations of the average partial Hertzian cone crack length (formed at the trailing edge of the probe) and average track width under different sliding contact conditions in the presence of DI water and GO dispersion. ....	102
<b>Figure 6.9</b> Column plot showing the variation of maximum tensile stress $\sigma_t$ and critical cone crack initiation load $P_c$ under sliding in DI water and GO dispersion environments as a function of applied normal load. The numbers represent the quantitative values of stress and critical load for each applied load. The hatched columns represent the corresponding values for GO-lubricated sliding conditions. ....	106
<b>Figure 6.10</b> Schematic showing the mechanism of GO tribofilm deposition under normal and shear stresses exerted by a sliding indenter over the silica glass substrate.....	107
<b>Figure 6.11</b> Column plot showing the variation of calculated fracture energy per crack (red) and the total energy dissipated per unit sliding length (blue) as a function of applied normal load in the presence of DI water and GO dispersion. The hatched columns represent the energy values for GO-lubricated sliding conditions.....	110

<b>Figure 6.12</b> (A) Images of SLS glass before (top) and after (bottom) GO coating deposition, (B) UV-visible transmission spectra of bare and GO-glasses, (C) Optical micrograph of the surface of GO-glass, (D) AFM topography map of the GO deposition, (E) Micro-Raman spectra of the pristine GO, bare SLS glass, and GO-glass.....	112
<b>Figure 6.13</b> Variation of the COF with sliding time for the bare SLS glass and the GO-glass at applied loads of 7, 10, and 15 N. ....	114
<b>Figure 6.14</b> The optical micrographs and cross-section profiles (across dotted lines) of the scratch tracks on GO-glass and bare SLS glass at loads of (A, B, C) 7 N, (D, E, F) 10 N, and (G, H, I) 15 N. ....	115
<b>Figure 7.1</b> Process flow of the steps involved in the mechanical exfoliation of graphene on silica glass surfaces.....	120
<b>Figure 7.2</b> The simulation model for static water-glass interactions without (A) and (B) with graphene at the interface, (C) The simulation model for dynamic interactions between a silicon slab (top) pressing and shearing against a silica glass block (bottom) with entrapped water molecules. Matching the static simulations, parallel dynamic simulations involving/excluding graphene were conducted.....	122
<b>Figure 7.3</b> (A) Gridded silica glass specimen used as the substrate for graphene exfoliation, (B) 100× optical micrograph of the exfoliated graphene sheets on the glass surface, (C) AFM topography, and (D) friction micrographs showing multi-layer and few-layer graphene deposition, (E) Extracted line profile showing the step height of an exemplar few-layer graphene sheet (shown in inset image) along the edge, (F) Micro-Raman spectra of graphene layers with an increasing thickness (bottom-to-top) along with their respective $I_{2D}/I_G$ ratios. ....	124
<b>Figure 7.4</b> (A) Schematic of the AFM scratch experimental setup, (B) Variation of friction force with normal load for glass and graphene-glass (inset shows the zoomed-in curve for graphene-glass before sheet rupture), (C) The AFM topography micrographs of the worn region post scratch experiments on glass (left) and graphene-glass (right), (D) The Z-axis line profiles corresponding to the dotted lines drawn across the scratched region as shown in (C). ....	129
<b>Figure 7.5</b> (A) Atomistic simulation model of scratch on the graphene-glass surface, (B) Load-displacement curves recorded during the indentation of glass and graphene-glass surfaces (inset shows the calculated elastic modulus and indentation hardness of both surfaces), (C) Simulated coefficient of friction (COF) with respect to the scratch distance for glass vs. graphene-glass	

surface, **(D)** Scratch morphologies of the underlying glass in the absence (left) and in the presence (right) of monolayer graphene (overlaid profile represents the depth for comparison), **(E)** Top view of the shear strain maps and **(F)** Side cross-sectional view of the volumetric strain maps comparing the glass response without vs. with monolayer graphene.

..... 133

**Figure 7.6** **(A)** The friction vs. normal load variation during the wet scratch tests on glass and graphene-glass (inset shows the zoomed-in plot for graphene-glass), the topography micrographs of the worn region over **(B)** glass and **(C)** graphene-glass surface (white dotted box represents the test region), the TGT-1 calibration grating profile of the diamond tip before **(D)** and after **(E)** wet scratch tests on the bare glass surface. .... 137

**Figure 7.7** **(A)** The friction vs. normal load variation during the wet scratch tests on glass and graphene-glass (inset shows the zoomed-in plot for graphene-glass), the topography micrographs of the worn region over **(B)** glass and **(C)** graphene-glass surface (white dotted box represents the test region), the TGT-1 calibration grating profile of the DLC tip before **(D)** and after **(E)** wet scratch tests on the bare glass surface. .... 141

**Figure 7.8** The evolution in the count of **(A)** Si—OH hydration bonds, and **(B)** Si—O—Si bridging bonds across the water-glass junction during the static and dynamic interactions, respectively, without/with graphene; the color maps representing the magnitudes of atomic displacement vectors after sliding the silicon tip against the **(C)** bare glass and the **(D)** graphene-glass in the presence of interfacial water. .... 145

**Figure 7.9** The variation in the frictional forces acting on the silicon tip while sliding against bare glass (blue) and graphene-glass (red). The light and dark lines represent the raw and time-averaged forces, respectively. .... 146

**Figure 8.1** **(A)** The experimental CVD setup for 2D materials growth, **(B)** Schematic of the deposition process of monolayer WS<sub>2</sub> on a silica glass substrate. .... 150

**Figure 8.2** **(A)** The silica glass specimen before (bottom) and after (top) the CVD growth of WS<sub>2</sub> film, **(B)** the AFM topography micrograph of WS<sub>2</sub>-glass surface, and **(C)** the corresponding friction micrograph showing the lateral force contrast between WS<sub>2</sub> and glass, **(D)** a 50× optical micrograph and **(E)** the corresponding fluorescence micrograph of the WS<sub>2</sub>-glass surface, and **(F)** 3D projection of the step height along the edge of monolayer WS<sub>2</sub> (overlay plot shows the extracted 2D line profile across the step region). .... 152

**Figure 8.3** (A) The micro-Raman spectra of monolayer WS<sub>2</sub> recorded at multiple locations, (B) XPS survey scan showing the presence of W, S, C, and O elements in the as-grown WS<sub>2</sub> monolayers, and the deconvoluted XPS spectrum of (C) W and (D) S. .... 153

**Figure 8.4** (A) Variation in the friction with the normal load applied during AFM scratching of the glass and WS<sub>2</sub>-glass surfaces (inset shows the zoomed-in WS<sub>2</sub>-glass plots along with the graphene-glass trend for comparison), the topography micrograph of the worn surface of (B) glass and (C) WS<sub>2</sub>-glass after scratch tests, (D) comparison of the linear cross-section profiles of the worn-out glass and deformed WS<sub>2</sub>-glass (extracted across dotted lines shown in panel B and C), and (E) the equivalent line profile comparison between deformed WS<sub>2</sub>-glass and graphene-glass..... 156

**Figure 8.5** (A) Atomistic model for scratch simulations on the WS<sub>2</sub>-glass surface, (B) top view of the scratch track terrain (left) and atomic shear strain (right) for the silica glass in the absence (top row) and the presence (bottom row) of protective monolayer WS<sub>2</sub> film, the X-section (C) and Y-section (D) topography profiles of WS<sub>2</sub>-glass assembly (extracted along the white and yellow dotted lines, respectively, in panel (B) showing the morphology of WS<sub>2</sub> and the underlying silica glass at the instances of peak indentation (t = 0 ps) and complete scratch (t = 750 ps), (E) cross-sectional densification map highlighting the local atomic densities in the subsurface region after the completion of scratch, and (F) the evolution of sheared (broken/switched) Si—O bond count with scratch distance (inset images represent bond breaking (top-left) and switching (bottom-right))..... 161

**Figure 8.6** The methodology of computing the sheared Si—O bonds in silica glass during scratch underneath WS<sub>2</sub>. The left images represent the two configurational snapshots (reference and current) which are compared at multiple timesteps. The reference frame is the peak indentation configuration, while the current frame is the instantaneous configuration at a particular timestep ‘N’ during scratch. A given Si—O bond is termed “sheared” when the near-coordination environment about the central Si atom is altered with respect to the reference frame. As shown in the diagram, bond switching involves the replacement of one/more of the coordinating oxygen, while bond breaking reduces the number of coordinating oxygen. .... 162